PERGAMON

Journal of Structural Geology 24 (2002) 297–309

JOURNAL OF STRUCTURAL GEOLOGY

www.elsevier.com/locate/jstrugeo

Flow and strain patterns at the terminations of tapered shear zones

Nibir Mandal[a], Susanta Kumar Samanta[a], Chandan Chakraborty[b,*]

[a]*Department of Geological Sciences, Jadavpur University, Calcutta 700032, India*
[b]*Geological Studies Unit, Indian Statistical Institute, 203 B.T. Road, Calcutta 700035, India*

Received 20 December 2000; revised 1 April 2001; accepted 9 May 2001

Abstract

With the help of corner flow theory, this paper numerically analyzes the deformation pattern at the terminations of tapered shear zones, the walls of which are rigid and move parallel to each other in opposite directions. The overall flow pattern is characterized by curvilinear particle paths that show convexity towards and opposite to the tapering direction respectively for low ($<5°$) and high ($>10°$) inclinations of the wall verging opposite to the sense of wall movement. In tapered shear zones there are two distinct fields of instantaneous shortening and extension parallel to the direction of wall movement. Numerical models reveal that the finite strain distributions are generally asymmetrical with larger strain concentration occurring near the wall verging opposite to sense of wall movement. The S-foliation trajectories show a curvilinear pattern, convexing against the tapering direction. The analysis of rotationality (vorticity) indicates that the sense of vorticity near the synthetically verging wall is reverse to the sense of wall movement; however W_k is one everywhere within the shear zone.

Keywords: Non-parallel walls; Simple shear; Ductile flow; Vorticity; Foliation

1. Introduction

Theoretical, experimental and field studies over several decades have led to a comprehensive understanding on the kinematics of *parallel-sided*, ductile shear zones. In such shear zones the strain profiles generally remain almost constant in differing transects through the zones. However, shear zones can show walls which converge and diverge, and this type of non-parallelism is commonly observed at the terminations of most natural shear zones (Ramsay and Huber, 1987, p. 595). The deformation near the tapering ends of these shear zones (hereafter called *tapered shear zone*) is essentially heterogeneous, and the nature of strain distribution is extremely complicated with complex, laterally variable strain profiles (Freund, 1974; Ramsay and Graham, 1970; Ramsay, 1980; Simpson, 1983; Ingles, 1986; Ramsay and Huber, 1987). The intricacy of the deformation pattern within tapered shear zones and its dissimilarity with that of parallel-sided shear zones can also be demonstrated by means of simple physical model experiments (Fig. 1). An appropriate deformation model that describes the heterogeneous flow within tapered shear zones is, however, still lacking (see Ramsay, 1980; Ramsay and Huber, 1987). This paper investigates the heterogeneous flow within tapered shear zones with special reference to particle paths, strain distribution pattern and foliation trajectories, using a simple continuum model.

The continuum-mechanics approach is a useful way for the study of macro-scale ductile shear zones (Cobbold, 1977; Ramsay, 1980). Several workers have applied continuum models to analyze the deformation patterns in large-scale, parallel-sided shear zones involving transpressional movement (Sanderson and Marchini, 1984; Fossen and Tikoff, 1993; Tikoff and Teyssier, 1994; Dutton, 1997; Jones et al., 1997). The results of numerical simulations based on these models conform well to the structural features observed in natural, analogous transpression zones (e.g. Dutton, 1997; Jones et al., 1997). This paper also uses the continuum approach but applies the corner flow theory to study the flow and strain patterns in ductile, tapered shear zones with rigid walls.

Corner flow model (Batchelor, 1967) was utilized by several workers to explain exhumation in convergent settings (Cowan and Silling, 1978) and emplacement of exotic blocks in mélange terranes (Cloos, 1982, 1984). To study the flow kinematics of tapered shear zones we have, however, slightly modified the corner flow model of Batchelor (1967) as enumerated in the following section. The modified model has been used for numerical simulations

* Corresponding author. Fax: +91-33-577-6680.
E-mail addresses: nibir@jugeo.clib0.ernet.in (N. Mandal), chandan@isical.ac.in (C. Chakraborty).

0191-8141/01/$ - see front matter
PII: S0191-8141(01)00065-7

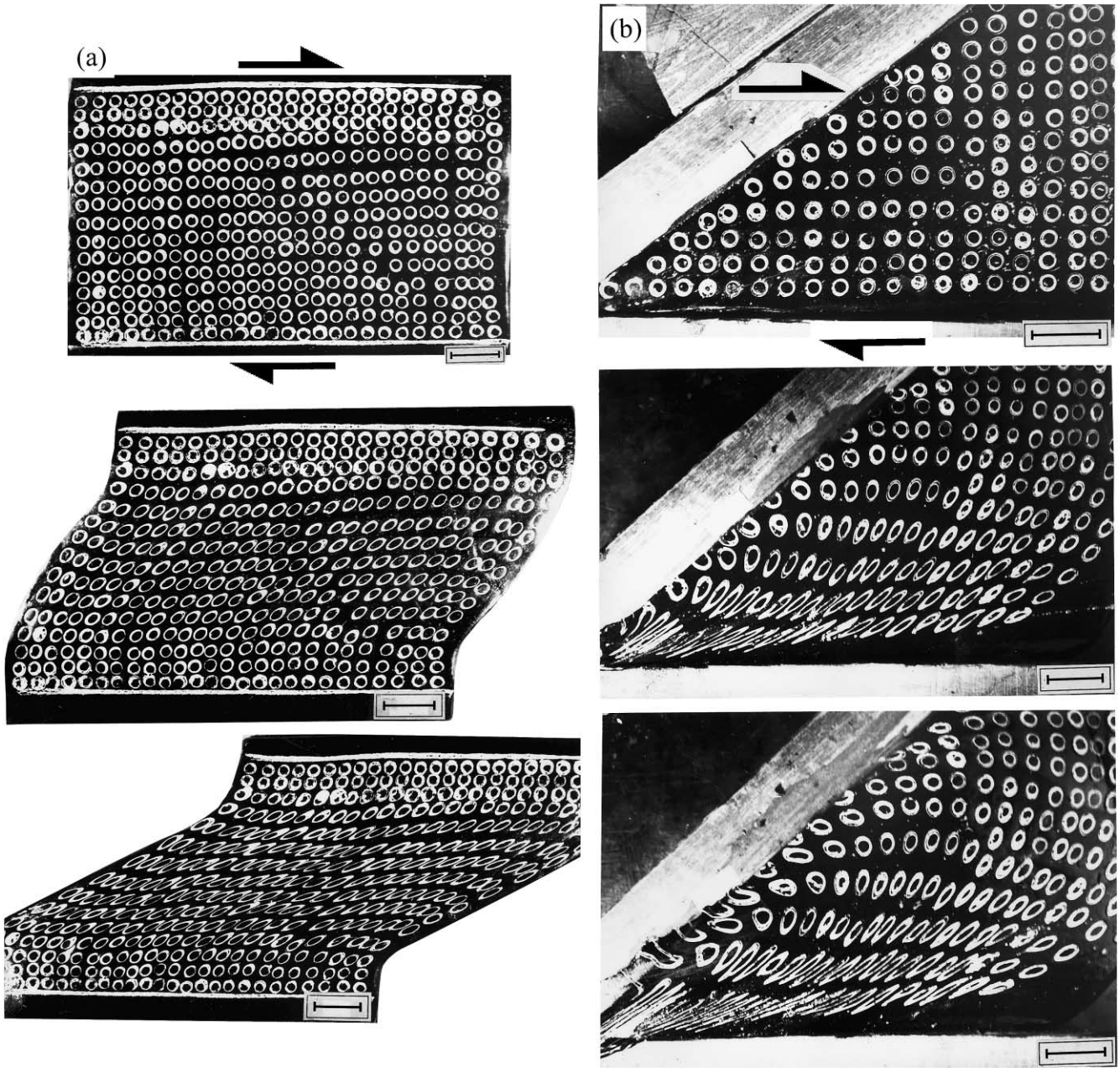

Fig. 1. Successive stages of physical model experiments on pitch blocks simulating the nature of strain distributions in parallel-sided (a) and tapered (b) shear zones. The sense of wall movements (dextral) are shown by arrows. In (b) one of the walls (bottom) was moved from right to left, keeping the other wall stationary. In the model of tapered shear zone (b) one wall is parallel to the movement direction, whereas the other wall is at a tilt of 35° with the movement direction. Note that: (1) such non-parallelism in shear zone geometry has resulted in asymmetrical strain distribution across the zone with the locale of high finite strains occurring near the wall parallel to the movement direction. (2) The vergence of *XY*-planes of strain ellipses with respect to the wall reverses across the shear zone. Scale bar = 2 cm.

of particle paths, strain distributions, vorticity fields and cleavage trajectories in tapered shear zones.

2. Theoretical consideration

2.1. The model

A tapered ductile shear zone is modeled by considering a slab of homogeneous viscous material within two non-parallel rigid plates simulating the shear zone walls. In the model the plates are displaced rectilinearly parallel to each other in opposite directions, and are inclined with synthetic and antithetic vergence with respect to the sense of wall movement (Fig. 2). Due to the rectilinear movement, the two opposite points on the boundaries of the shear zone at any transect show parallel displacements, and thereby maintain a constant distance measured normal to the

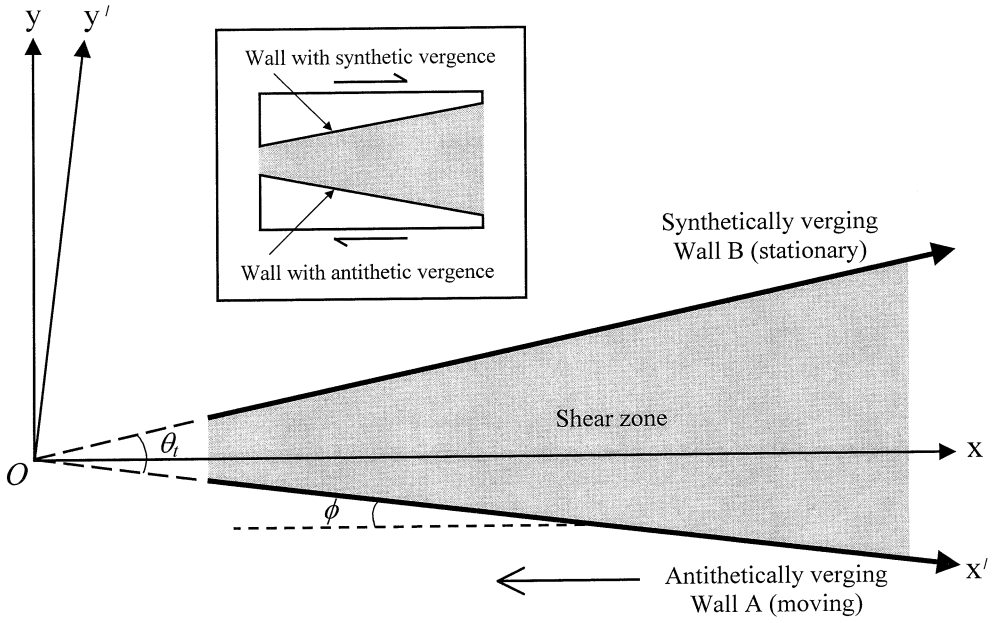

Fig. 2. Consideration of Cartesian coordinate frames for theoretical analysis of deformation in tapered shear zones (shaded) with non-parallel walls (A and B) undergoing parallel movements dextrally, as shown in the inset. The vergence of A and B with respect to the movement direction is in the opposite (antithetic) and same (synthetic) sense with respect to the sense of wall movement (dextral), respectively. θ_t is the taper angle between the walls and ϕ is the inclination of antithetically verging wall (A) with the movement direction. The antithetically and synthetically verging walls are considered as moving and stationary, respectively, for the calculations in numerical models.

movement direction as occurs in simple shear. The viscous material is considered to be perfectly welded with the rigid plates so that a non-slip boundary condition prevails at the shear zone wall (cf. Dutton, 1997). The movement of the plates thus induces flow in the viscous material between the plates. The analysis also assumes that there is no net volume loss or material accretion in the shear zone during the deformation.

2.2. Mathematical derivations

Consider a shear zone with non-parallel, rigid walls A and B, tapering at an angle θ_t, undergoing movement in a dextral sense (Fig. 2). In Batchelor's (1967) corner flow model one of the walls is considered to be disposed parallel to the movement direction and the other with a synthetic vergence. We, however, consider a general case with one of the plates verging antithetically (A) and the other synthetically (B) (Fig. 2), and therefore re-derive the equations in the following way. Let us choose a Cartesian frame Oxy with the origin at the converging point of the walls A, B, and x-axis parallel to the movement direction of the walls (Fig. 2). The wall A is at an angle ϕ with the x-axis, and moves at a velocity $-U$ along the x-axis relative to the wall B. Another Cartesian frame $Ox'y'$ is chosen with the x'-axis along the wall A. The instantaneous flow field within the shear zone can be described in terms of polar co-ordinates (r, θ) with respect to $Ox'y'$ frame as:

$$u_r = \frac{1}{r}\frac{\delta \Psi}{\delta \theta} \tag{1a}$$

$$u_\theta = -\frac{\delta \Psi}{\delta r} \tag{1b}$$

where u_r and u_θ are the radial and tangential velocity components, respectively. Ψ is the stream function, the expression of which must satisfy the following conditions.

At $\theta = 0$,

$$\frac{1}{r}\frac{\delta \Psi}{\delta \theta} = -U\cos\phi \tag{2a}$$

$$\frac{\delta \Psi}{\delta r} = U\sin\phi \tag{2b}$$

and at $\theta = \theta_t$,

$$\frac{1}{r}\frac{\delta \Psi}{\delta \theta} = 0 \tag{3a}$$

$$\frac{\delta \Psi}{\delta r} = 0 \tag{3b}$$

To satisfy the conditions in Eqs. (2a), (2b), (3a) and (3b) the stream function can be written in the form:

$$\Psi = rf(\theta) \tag{4}$$

(Batchelor, 1967). The equation of mass conservation in a flow is:

$$\nabla^2(\nabla^2 \Psi) = 0 \tag{5}$$

Substituting the expression of Ψ (Eq. (4)) in Eq. (5),

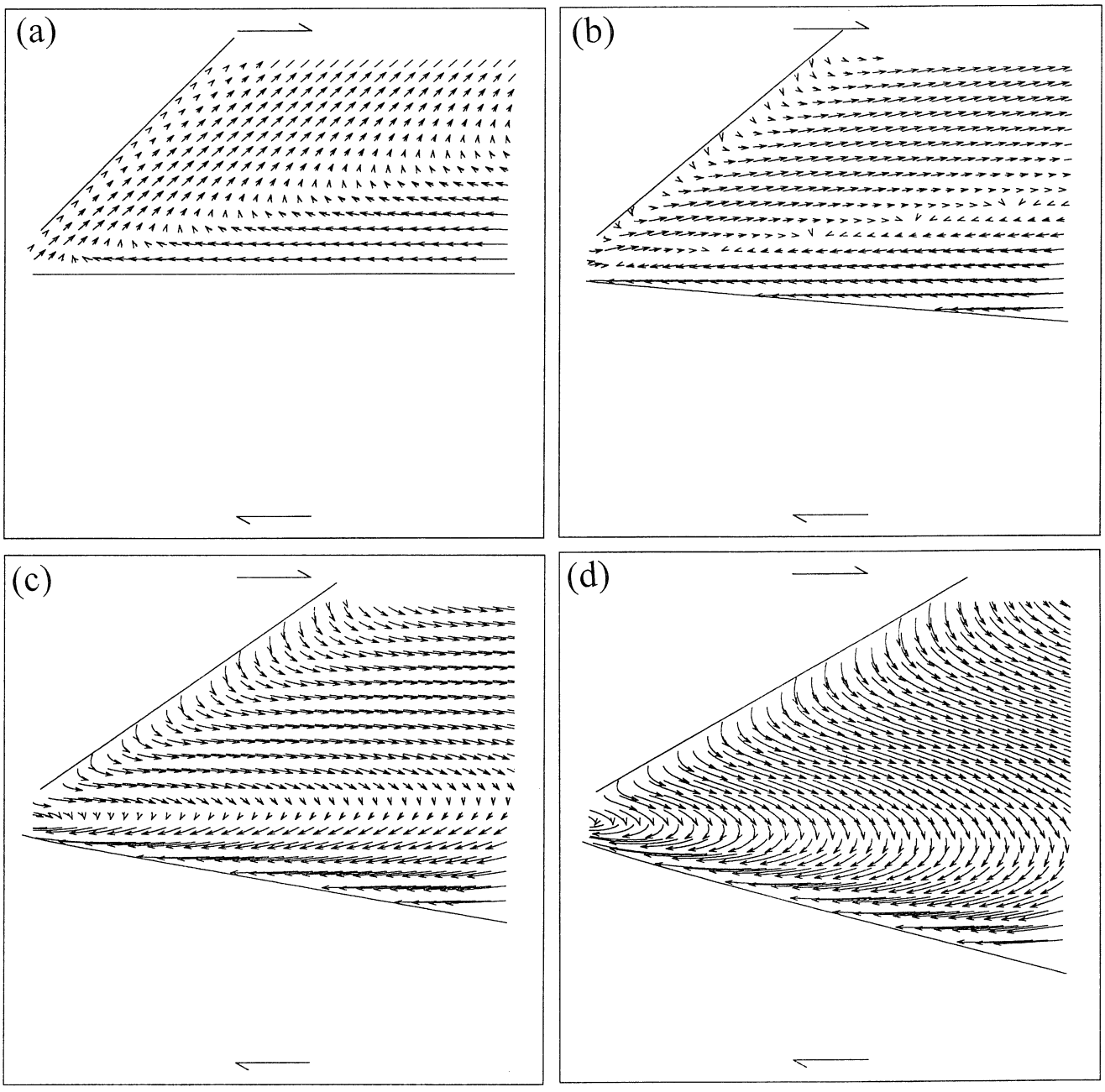

Fig. 3. Flow patterns in non-parallel, dextral shear zones with taper angle $\theta_t = 45°$. $\phi = 0$, 5, 10 and 15° in (a)–(d), respectively. See text for details.

we have:

$$\nabla^2\left[\frac{1}{r}(f + f'')\right] = \frac{1}{r^3}\left(f + f'' + f^{iv}\right) = 0 \tag{6}$$

The primes indicate the order of differentiation of the function f. The expression of f that fulfils Eq. (6) is:

$$f(\theta) = A\sin\theta + B\cos\theta + C\theta\sin\theta + D\theta\cos\theta \tag{7}$$

A, B, C and D are constants, the expressions of which need to be determined by applying the boundary conditions in Eqs. (2a), (2b), (3a) and (3b). Substituting the expression of f (Eq. (7)) in Eq. (4) and putting the derivative expression in Eqs. (1a) and (1b), we get:

$$u_r = f'(\theta) = A\cos\theta - B\sin\theta + C(\sin\theta + \theta\cos\theta) + D(\cos\theta - \theta\sin\theta) \tag{8a}$$

$$u_\theta = -f(\theta) = -(A\sin\theta + B\cos\theta + C\theta\sin\theta + D\theta\cos\theta) \tag{8b}$$

Replacing $\theta = 0$ in Eqs. (8a) and (8b) and then comparing

with Eqs. (2a) and (2b), it follows that:

$$A + D = -U\cos\phi \tag{9a}$$

$$B = U\sin\phi \tag{9b}$$

Similarly, by applying the conditions at $\theta = \theta_t$ (Eqs. (3a) and (3b)) we get:

$$A\cos\theta_t - B\sin\theta_t + C(\sin\theta_t + \theta\cos\theta_t) + D(\cos\theta_t - \theta_t\sin\theta_t) = 0 \tag{9c}$$

$$A\sin\theta_t + B\cos\theta_t + C\theta_t\sin\theta_t + D\theta_t\cos\theta_t = 0 \tag{9d}$$

Solving Eqs. (9a)–(9d), we find:

$$A = \frac{U}{\sin^2\theta_t}\left[\cos^2\theta_t\cos\phi - K\left(\theta_t + \sin\theta_t\cos\theta_t\right)\right] \tag{10a}$$

$$B = U\sin\phi \tag{10b}$$

$$C = UK \tag{10c}$$

$$D = -\left[\cos\phi + \frac{1}{\sin^2\theta_t}\left\{\cos^2\theta_t\cos\phi - K\left(\theta_t + \sin\theta_t\cos\theta_t\right)\right\}\right]U \tag{10d}$$

where

$$K = \frac{\theta_t - \sin\theta_t\cos\theta_t\left\{(1-\theta_t)^2\cos\phi + \theta_t^2\right\} + \sin^2\theta_t\{\theta_t(\cos\phi - 1) + \sin\phi\}}{\theta_t^2 - \sin^2\theta_t}$$

It may be noted that the expressions of the constants in Eqs. (10a)–(10d) are identical to those given by Batchelor (1967) if the wall A is considered to be disposed parallel to its movement direction (i.e. $\phi = 0$, Fig. 2).

Now, the instantaneous velocity at a point in the reference frame Oxy can be determined along the following steps. First, the Cartesian co-ordinate of the point (x, y) is transformed into the $Ox'y'$ space by:

$$\begin{bmatrix} x' \\ y' \end{bmatrix} = \begin{bmatrix} \cos\phi & \sin\phi \\ -\sin\phi & \cos\phi \end{bmatrix}\begin{bmatrix} x \\ y \end{bmatrix} \tag{11}$$

As the velocity functions are defined in terms of polar coordinates in $Ox'y'$ frame, the position of the point is expressed by r and θ, where $r = \sqrt{x'^2 + y'^2}$ and $\tan\theta = (y'/x')$ and to find the velocity vector with respect to Oxy frame we need to exercise the following conversion:

$$\begin{bmatrix} u \\ v \end{bmatrix} = \begin{bmatrix} \cos\phi & -\sin\phi \\ \sin\phi & \cos\phi \end{bmatrix}\begin{bmatrix} u_r \\ u_\theta \end{bmatrix} \tag{12}$$

Eqs. (10a)–(10d) indicate that the constants in the velocity functions (Eqs. (8a)–(8b)) depend upon two parameters: (i) the taper angle (θ_t) of shear zone walls, and (ii) the orientation of the shear zone walls with respect to their direction of movement (ϕ). For given values of θ_t and ϕ the instantaneous velocity vector at any point can be determined readily from Eqs. (8)–(12). Utilizing these equations we performed sets of numerical model experiments to study the flow patterns, vorticity and strain distributions in tapered shear zones.

3. Numerical models

3.1. Flow pattern

The kinematics of ductile shear zones is appositely reflected by the particle paths. In parallel-sided shear zones the flow is represented by rectilinear particle paths under simple shear and hyperbolic paths in a combination of simple and pure shears (Ramberg, 1975). However, in tapered shear zones, although the relative motion of walls is rectilinear, the particle paths of ductile flow within the shear zone are likely to be complex due to non-parallelism of the walls, as revealed in the following numerical experiments.

We simulated particle paths, as is conventionally done, by considering stepwise displacements of material points for a large number of increments in bulk shear. After each increment, the reference frame $Ox'y'$ was repositioned so that its origin remains in coincidence with the meeting point of the shear zone walls A and B. A set of experiments was performed by varying the orientation of the antithetically verging wall (ϕ) with respect to the movement direction. The experiments reveal that flow patterns within tapered shear zones are distinctly different from those of parallel-sided shear zones.

When ϕ is 0°, particles take a turn as they move in the tapering direction of the shear zone, describing a vortex flow pattern (Fig. 3a; cf. Batchelor, 1967). The line along which particles reverse their movement direction is asymmetrically oriented with respect to the two non-parallel walls, and is closer to the wall verging opposite to the sense of wall movement. Particles on either side of this line describe nearly rectilinear paths parallel to the shear zone walls. With a slight increase in ϕ value (5°) the vortex flow pattern is replaced by a more or less laminar flow pattern with parallel-disposed particle paths defining two zones within which the movement direction is opposite; the particle paths are, however, oblique to both the shear zone walls, but are nearly parallel to the direction of wall movement (Fig. 3b). When ϕ is further increased (10°), the flow pattern is significantly different from the earlier ones (Fig. 3c). Particles adjacent to the synthetically verging wall follow curved paths, convexing in the tapering direction of the shear zone, and then becoming nearly parallel to the

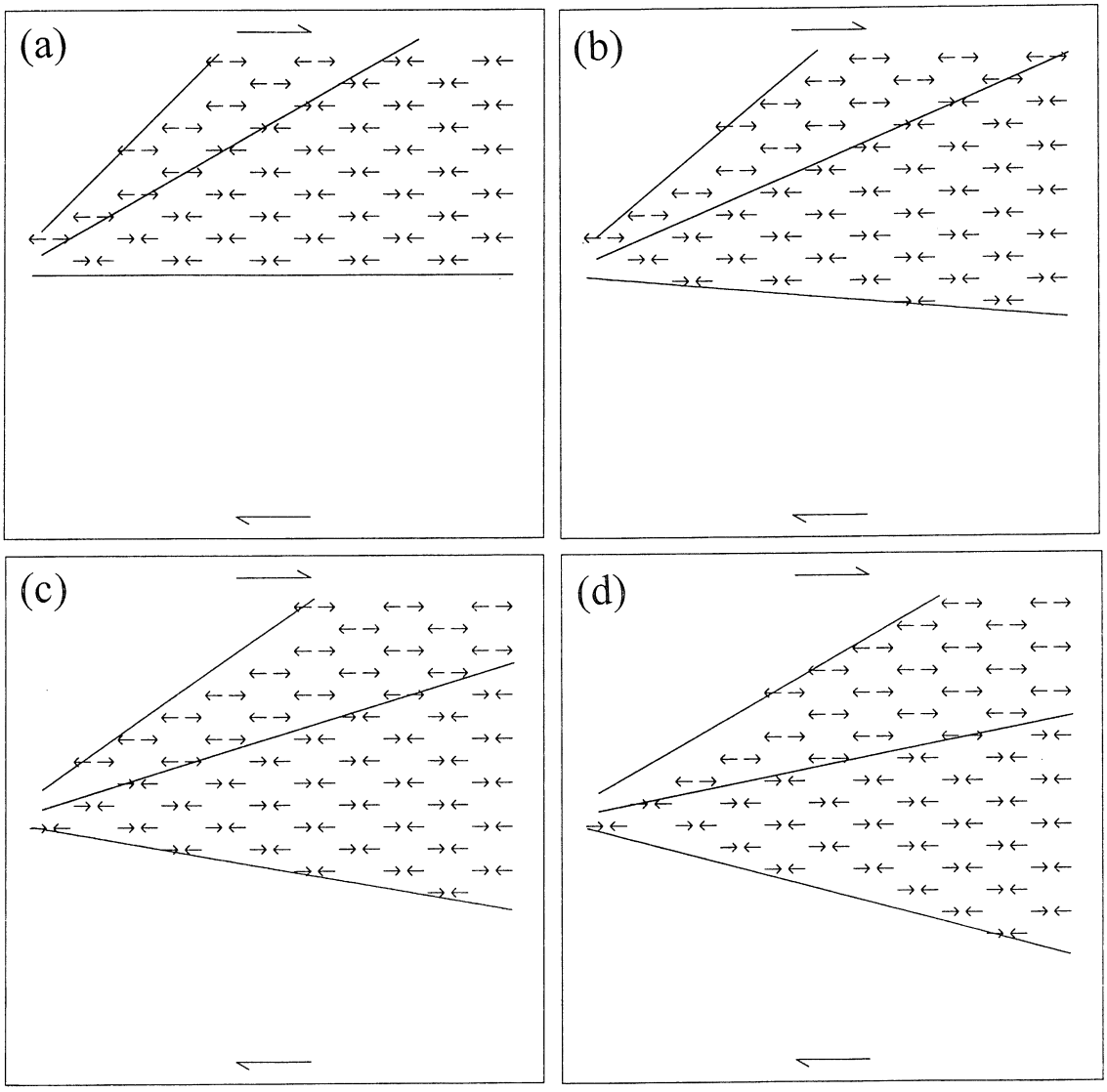

Fig. 4. Fields of shear-parallel instantaneous shortening (arrows heading towards each other) and extension (arrows heading away from each other) in tapered shear zones. Solid lines within the shear zone divide the two fields. The geometric conditions are the same as in Fig. 3.

direction of wall movement. On the other hand, particles near the antithetically verging wall describe curved paths convexing away from the tapering direction (Fig. 3c). At $\phi = 15°$ (Fig. 3d), the pattern of particle paths is similar to that of the previous model. However, the paths everywhere are in general oblique to the bulk shear direction. Experiments reveal that the flow patterns described above do not change significantly when the taper angle (θ_t) is varied, keeping ϕ constant.

It follows that the particle paths in tapered shear zones deviate discernibly from the rectilinear pattern characteristic of parallel-sided shear zones undergoing simple shear movement, and are sensitive to the inclination of the antithetically verging wall with respect to its movement direction.

3.2. Strain analysis

Ramsay and Graham (1970) have modelled the nature of strain variations across parallel-sided shear zones and shown that the strain profiles are typically symmetric and do not vary laterally. To study the effect of non-parallelism of shear zone walls on the strain pattern we ran numerical experiments based on the theoretical model described earlier, which revealed significantly different strain distribution patterns from that of parallel-sided shear zones.

The infinitesimal strain at a point within a tapered shear zone can be described by its components with respect to polar coordinates (r, θ) as:

$$\epsilon_{rr} = \frac{\delta u}{\delta r} \tag{13a}$$

$$\epsilon_{\theta\theta} = \frac{u_r}{r} + \frac{1}{r}\frac{\delta u_r}{\delta \theta} \tag{13b}$$

$$\epsilon_{r\theta} = \frac{r}{2}\frac{\delta}{\delta r}\left(\frac{u_\theta}{r}\right) + \frac{1}{2r}\frac{\delta u_r}{\delta \theta} \tag{13c}$$

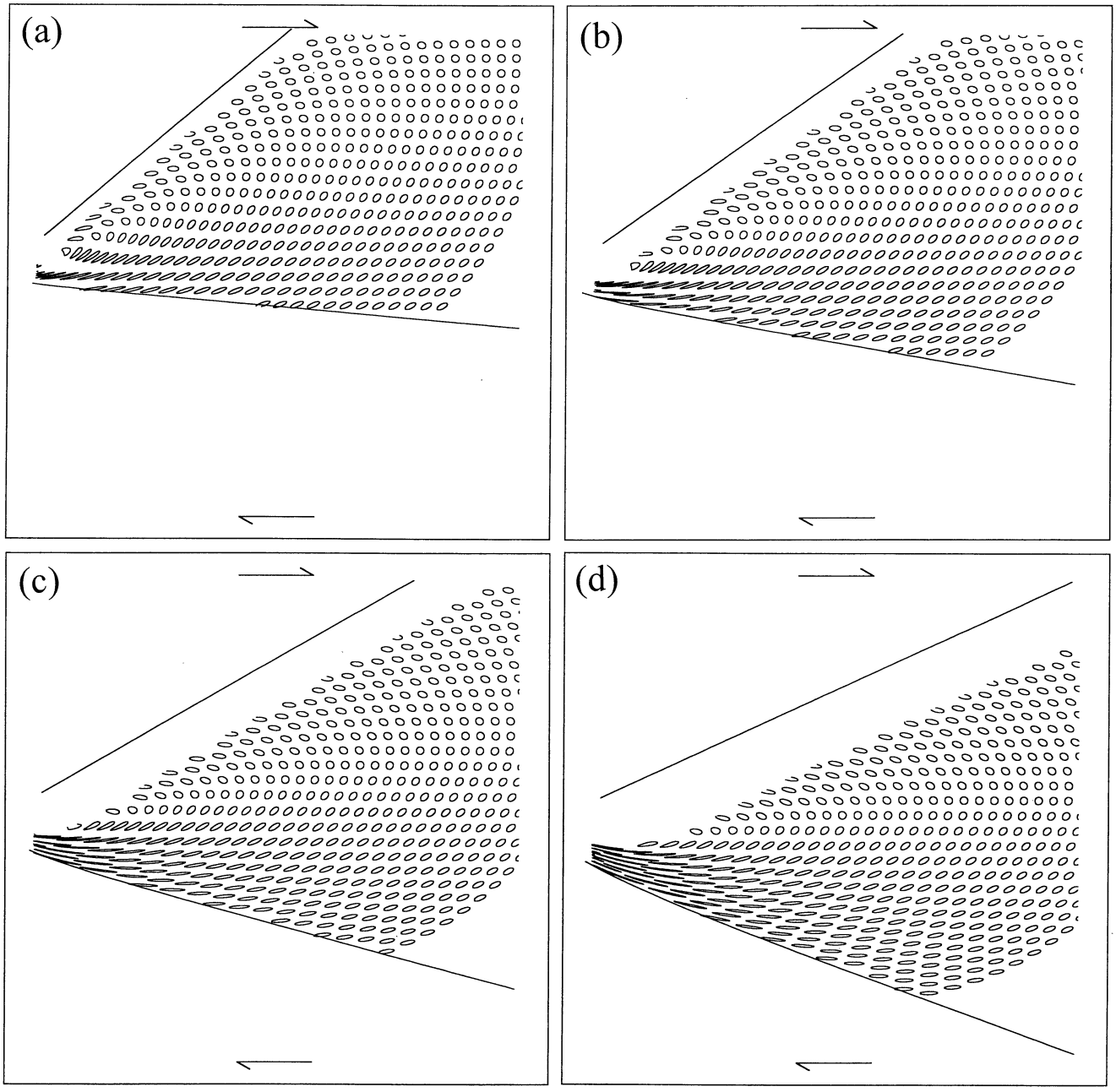

Fig. 5. Finite strain distributions in tapered shear zones with different inclinations (ϕ) of the antithetically verging (moving) wall. $\phi = 5$, 10, 15 and 20° in (a)–(d), respectively.

It can be shown from Eqs. (13a)–(13c) that there exists a component of longitudinal strain along the bulk shear direction (ϵ_{xx}), which has a relation with the strain components in Eqs. (13a)–(13c) as:

$$\epsilon_{xx} = \epsilon_{rr}\cos^2\theta - \epsilon_{r\theta}\sin\theta\cos\theta + \epsilon_{\theta\theta}\sin^2\theta \tag{14}$$

Substituting the expressions of u_r and u_θ (Eqs. (8a) and (8b)) in Eqs. (13a)–(13c) and replacing the derivative expression in Eq. (14), we get:

$$\epsilon_{xx} = \frac{1}{2r}(D\sin\theta - C\cos\theta)\sin 2\theta \tag{15}$$

Eq. (15) indicates that non-parallel disposition of shear zone walls can give rise to longitudinal strains parallel to the movement direction of the walls, defining fields of shear-parallel extension and shortening in the shear zone (Fig. 4). The field of shear-parallel shortening lies on the side of the antithetically verging wall, whereas the field of shear-parallel extension occurs near the other wall. The line separating the two fields is inclined to both the walls (Eq. (15)) and the angle with the antithetically verging wall can be given by:

$$\theta_c = \tan^{-1}\left(\frac{C}{D}\right) \tag{16}$$

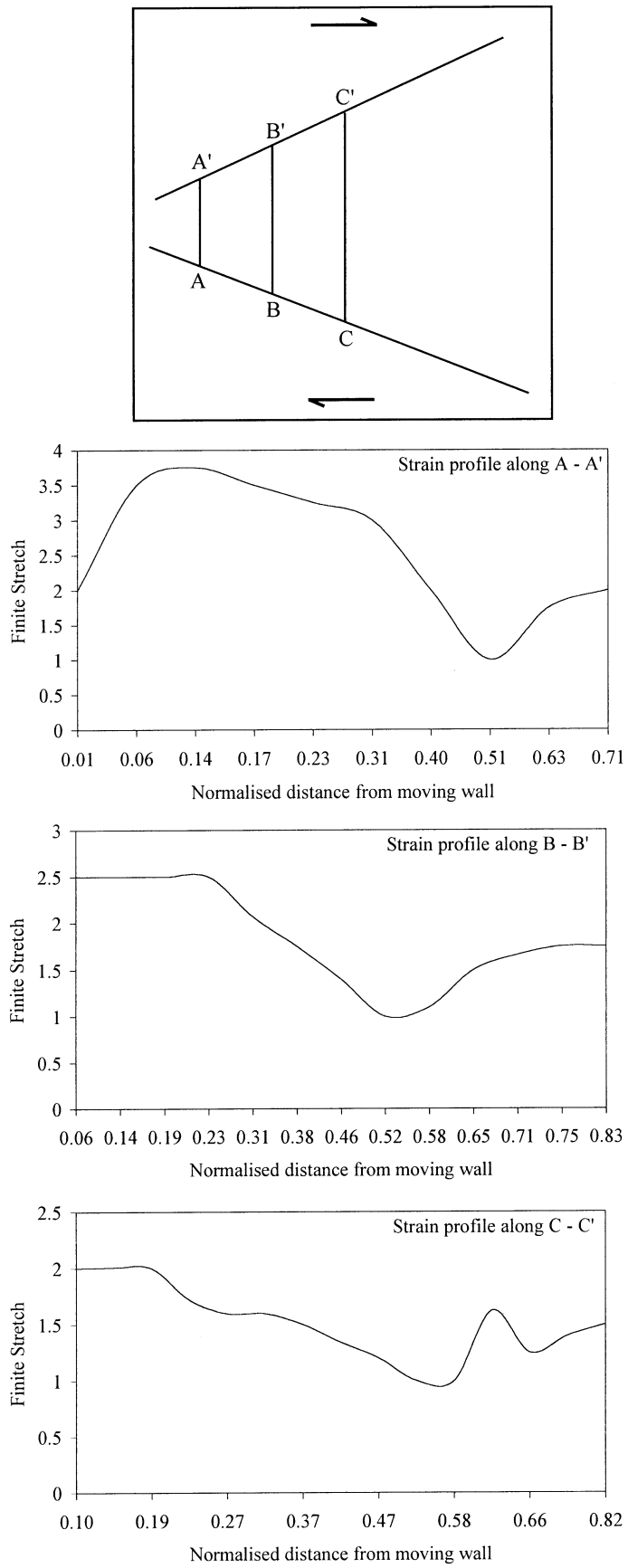

Fig. 6. Strain profiles along different sections in a tapered shear zone with taper angle $\theta_t = 45°$ and inclination of moving wall $\phi = 20°$.

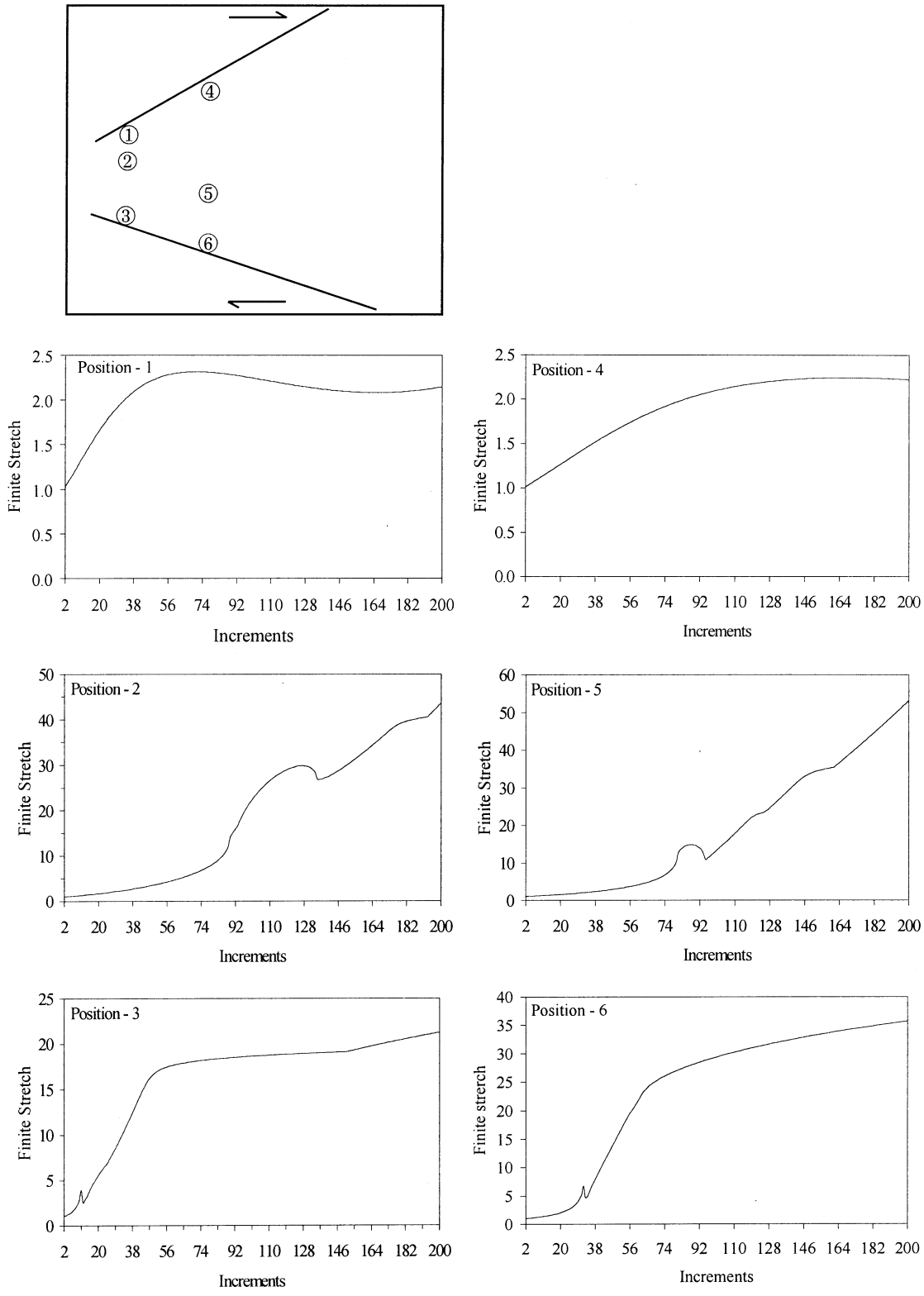

Fig. 7. Strain paths at different locations within a tapered shear zone. $\theta_t = 45°$ and $\phi = 20°$.

where the constants C and D are functions of taper angle (θ_t) and inclination of the antithetically verging wall with respect to the bulk shear direction (ϕ). For a given taper angle, with increase in ϕ, θ_c increases, resulting in relative expansion of the field of shear-parallel shortening (Fig. 4d).

A set of numerical model experiments was run to study the finite strain distribution in tapered shear zones. The

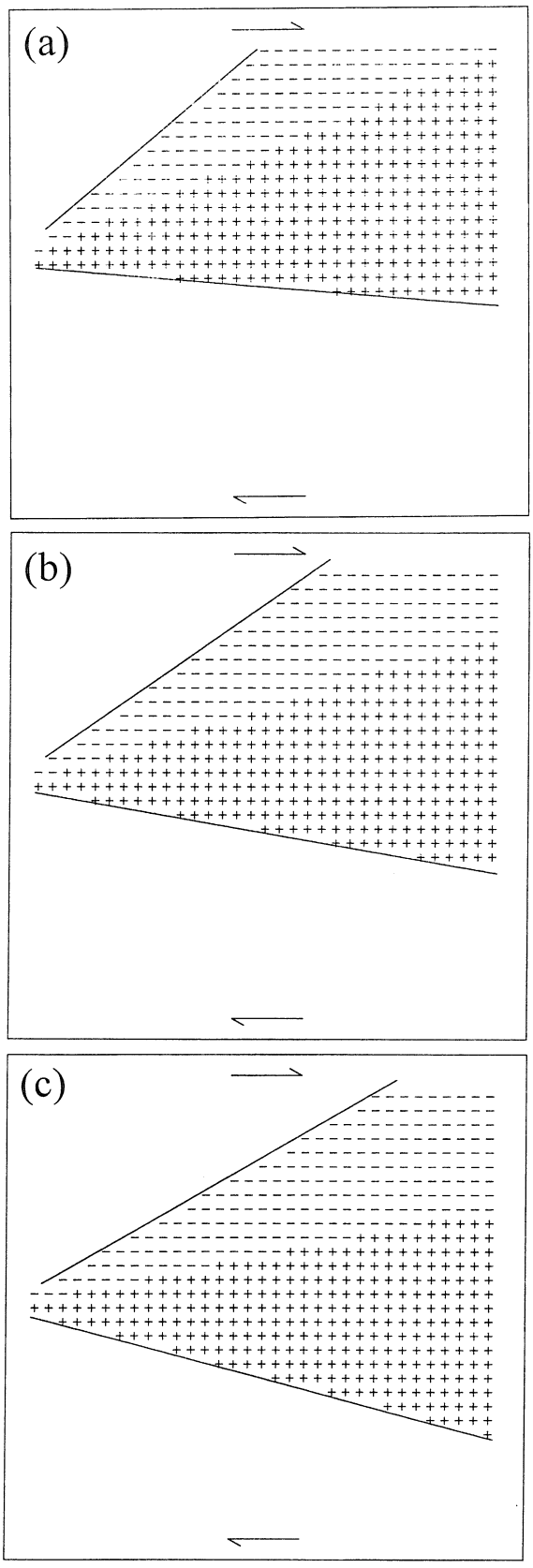

Fig. 8. Fields of synthetic (plus) and antithetic (dashed) vorticity (rotationality) in non-parallel shear zones with different inclinations (ϕ) of the moving wall. $\phi = 5$, 10 and 15° in (a)–(c), respectively.

model initially had small, circular markers in a Cartesian grid with respect to the *Oxy* reference frame, which are deformed into ellipses of different shapes and orientations reflecting a heterogeneous strain field within the shear zone. The experiments were performed for different inclinations of the antithetically verging wall (ϕ), keeping the taper-angle of the shear zone walls constant.

Models show an asymmetrical strain distribution with respect to the shear direction (Fig. 5) as observed in the physical model experiments (Fig. 1b). There is also preferential localization of high finite strain along the two walls of the shear zone with an intervening low-strain zone (Fig. 5). The finite strains near the wall verging opposite to the sense of wall movement are, however, larger compared with that near the wall verging in the same sense.

The vergence of strain ellipses is, in general, consistent with the sense of wall movement near the antithetically verging wall, whereas that close to the synthetically verging wall is in the opposite sense (Fig. 5). However, at higher values of ϕ (20°) the strain ellipses near the antithetically verging wall tend to verge opposite to the sense of wall movement, particularly in the tapering region (Fig. 5d). With increase in ϕ, an overall widening of high-strain zone associated with the antithetically verging wall is also noticed (Fig. 5).

Field studies reveal that strain profiles in tapered shear zones are generally asymmetrical, showing ups and downs, and the shape of the profile also varies laterally (Simpson, 1983). Similar types of strain profiles are obtained in our numerical models, characterized by a valley with peaks and plateaus on either side (Fig. 6).

We also ran a set of numerical experiments to investigate the nature of strain paths at different locations within a shear zone. The results show that the temporal variation in finite strain is different at different locations. The strain at points located near the synthetically verging wall increases to a maximum, then drops slightly to a minimum, and finally increases with a gentle gradient (Fig. 7). In contrast, at points in the central region there is an unsteady increase in the finite strain resulting in irregular strain paths (Fig. 7). The finite strain at points near the antithetically verging wall increases steeply along a linear path barring a small perturbation, and subsequently increases at a much slower rate (Fig. 7).

3.3. Vorticity field

Vorticity, a measure of rotationality of non-coaxial deformation, can be used to analyze the sense of local shear and the magnitude of rotationality in tapered shear zones. This can be described in terms of polar co-ordinates as:

$$W = \nabla \times u = \left[\frac{1}{r} \frac{\delta(r u_\theta)}{\delta r} - \frac{1}{r} \frac{\delta u_r}{\delta \theta} \right] \tag{17}$$

Substituting the expressions of u_r and u_θ (Eqs. (8a) and (8b))

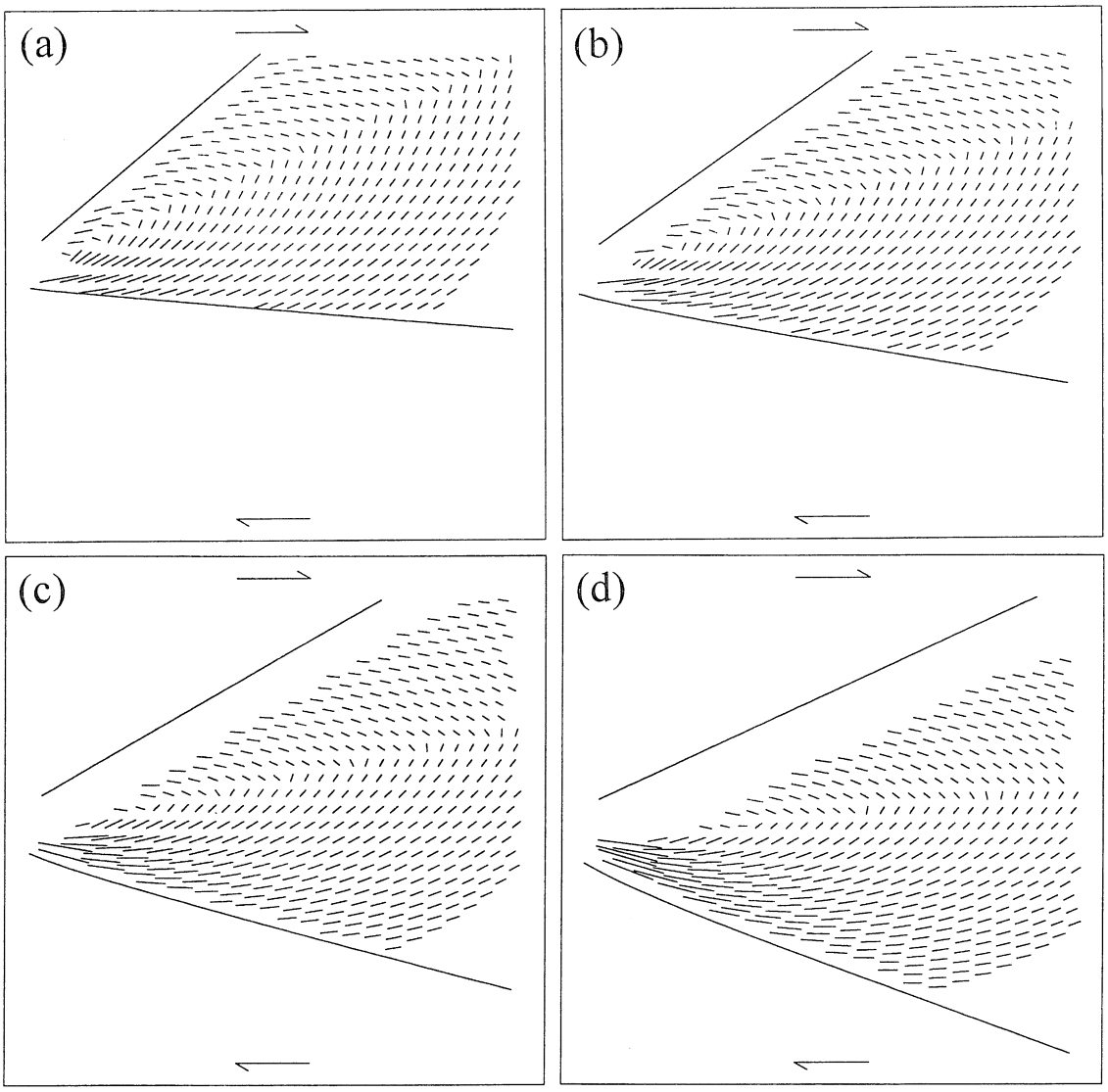

Fig. 9. Trajectories of S-foliations in tapering shear zones. $\phi = 5$, 10, 15 and 20° in (a)–(d), respectively. Taper angle $\theta_t = 45°$.

in Eq. (17), we have:

$$W = \frac{2}{r}(D \sin \theta - C \cos \theta) \tag{18}$$

Eq. (18) shows that irrespective of r the vorticity is zero at a critical value of θ:

$$\theta_c = \tan^{-1} \frac{C}{D} \tag{19}$$

A line making an inclination θ_c with the antithetically verging wall divides the flow field within the shear zone into two quadrants. In the quadrant with $\theta < \theta_c$ the sense of local shear is synthetic, whereas that in the quadrant with $\theta > \theta_c$ is antithetic with respect to the sense of wall movement. The taper angle (θ_t) and the orientation (ϕ) of the shear zone walls seem to be the principal parameters in determining the areal proportions of the fields of synthetic and antithetic shear. Using Eq. (18) a set of numerical experiments was performed by varying the inclination of the wall verging antithetically to the sense of wall movement at a constant taper angle of 45°. With increase in ϕ the field of antithetic shear tends to enlarge at the expense of the field of synthetic shear (Fig. 8).

The kinematical vorticity number W_k is used as a measure of non-coaxiality (Truesdell, 1954; Means et al., 1980), the expression of which in plane strain condition is:

$$W_k = \frac{W}{\sqrt{2(\epsilon_1^2 + \epsilon_2^2)}} \tag{20}$$

where ϵ_1 and ϵ_2 are the principal stretch rates. If the deformation does not involve any volume loss, i.e. $\epsilon_1 + \epsilon_2 = 0$, Eq. (20) simplifies to:

$$W_k = \frac{W}{2\epsilon_1} \tag{21}$$

ϵ_1 has the relation with the strain rate components defined in polar coordinates as $\epsilon_1 = \sqrt{\epsilon_{r\theta}^2 - \epsilon_{rr}\epsilon_{\theta\theta}}$. Since $\epsilon_{rr} + \epsilon_{\theta\theta} = 0$, $\epsilon_1 = \sqrt{\epsilon_{r\theta}^2 + \epsilon_{rr}^2}$. Substituting the expression of ϵ_1 in Eq. (21), you get:

$$W_k = \frac{W}{2\sqrt{\epsilon_{r\theta}^2 + \epsilon_{rr}^2}} \tag{22}$$

In the present case $\epsilon_{rr} = 0$. Substituting the expressions of W and $\epsilon_{r\theta}$ we find that the magnitude of W_k is always one. Thus, even if the walls of a shear zone are non-parallel the nature of local deformation within the shear zone is essentially of simple shear type, provided the walls move parallel to each other, simulating a simple shear type of bulk deformation.

3.4. Foliation trajectories

In ductile shear zones S-foliations develop tracking the *XY* planes of finite strain ellipses, and show curvilinear trajectories reflecting the nature of strain variation across the shear zone (Ramsay and Huber, 1987). In parallel-sided shear zones, the curvature of the trajectories varies systematically in a symmetrical manner across the shear zone. Moreover, the vergence of the foliations with respect to the shear zone walls remain the same everywhere. It is, however, apparent from the physical model experiments (Fig. 1) that the foliation trajectories in tapered shear zones would be much more complex, as is also revealed in the numerical models described below.

Numerical models were designed to track the S-foliations developing along the *XY* principal planes of finite strain ellipses under the heterogeneous flow field in tapered shear zones. Numerical experiments run at different inclinations of the antithetically verging wall with respect to its movement direction show that the foliation trajectories describe an overall curvilinear pattern convexing opposite to the tapering direction of the shear zone (Fig. 9). However, the vergence of the foliations with the respect to the sense of bulk shear is different in different domains of the shear zone (Fig. 9). Near the wall verging synthetically the foliations in general verge opposite to the sense of wall movement, whereas the foliation in the rest of the shear zone verge in the same sense. However, as the inclination of the wall verging antithetically is increased the foliation at the corner zone tends to verge opposite to the sense of bulk shear (Fig. 9d).

4. Summary

The principal findings of the present investigation can be summarized along the following points. (1) The corner flow theory of fluid mechanics can be utilized to study the deformation in shear zones with non-parallel walls. (2) Non-parallel disposition of the shear zone walls, as often noticed in nature, results in complex flow within the shear zone, markedly different from that in parallel-sided shear zones. (3) The flow pattern is largely controlled by the inclination of shear zone walls with respect to their movement direction. When the antithetically verging wall is at low inclination with the bulk shear direction, the ductile flow within the shear zone is represented by curvilinear particle paths, convexing in the tapering direction (Fig. 3a and b). With an increase in this inclination, particle paths also show convexity opposite to the tapering direction (Fig. 3c and d). (4) In ductile shear zones with non-parallel walls there are two fields showing instantaneous shortening and extension parallel to the movement direction of the walls. The field of shear-parallel extension occurs on the side of the wall verging opposite to the sense of movement of the walls (Fig. 4). (5) The finite-strain distribution in tapering shear zones is characteristically asymmetrical, showing high-strain zones along the wall verging antithetically (Fig. 5). (6) Non-parallel geometry of shear zone walls results in reversal of the vorticity sense. There is a line of particular orientation that divides the fields of synthetic and antithetic vorticity. The kinematical vorticity number W_k everywhere within the shear zone is, however, one (Fig. 8). (7) S-foliations in tapered shear zones can show an opposite sense of obliquity with the walls on either side of the shear zone (Fig. 9).

In the present model there are certain simplistic assumptions: (i) the model is two-dimensional, based on plane strain condition; (ii) it does not take into account any effect of volume change, which has been reported from natural shear zones (Mohanty and Ramsay, 1994; Ring, 1999); (iii) the shear zone walls are assumed to be rigid, and perfectly welded to the ductile rock within the shear zone; and (iv) in the analysis one wall is moved, keeping the other wall stationary; if both the walls were assumed to be moving, particle paths would be different from that presented here, however, the patterns of strain distribution and associated structures in the shear zone would remain qualitatively the same.

Acknowledgements

We wish to thank Professors W.M. Schwerdtner, C. Teyssier and C.W. Passchier for their comments that greatly contributed to the improvement of the paper. We are grateful to DST, India for extending a financial support. CC acknowledges the infrastructural facilities provided by the Indian Statistical Institute, Calcutta.

References

Batchelor, G.K., 1967. An Introduction to Fluid Dynamics. The University Press, Cambridge, 615pp.

Cloos, M., 1982. Flow melanges: numerical modelling and geologic

constraints on their origin in the Franciscan subduction complex, California. Geological Society of America Bulletin 93, 330–345.

Cloos, M., 1984. Flow melanges and the structural evolution of accretionary wedges. Geological Society of America Special Paper 198, 71–79.

Cobbold, P.R., 1977. Description and origin of banded deformation structures. I. Regional strain, local perturbations and deformation bands. Canadian Journal of Earth Sciences 14, 1721–1731.

Cowan, D.S., Silling, R.M., 1978. A dynamic, scaled model of accretion at trenches and its implications for the tectonic evolution of subduction complexes. Journal of Geophysical Research 83, 5389–5396.

Dutton, B.J., 1997. Finite strains in transpression zones with no boundary slip. Journal of Structural Geology 19, 1189–1200.

Fossen, H., Tikoff, B., 1993. The deformation matrix for simultaneous pure shear, simple shear, and volume change, and its application to transpression/transtension tectonics. Journal of Structural Geology 15, 413–422.

Freund, R., 1974. Kinematics of transform and transcurrent faults. Tectonophysics 21, 93–134.

Ingles, J., 1986. Terminations of ductile shear zones. Tectonophysics 127, 87–95.

Jones, R.R., Holdswarth, R.E., Bailey, W., 1997. Lateral extrusion in transpression zones: the importance of boundary conditions. Journal of Structural Geology 19, 1201–1217.

Means, W.D., Hobbs, B.E., Lister, G.S., Williams, P.F., 1980. Vorticity and non-coaxiality in progressive deformations. Journal of Structural Geology 2, 371–378.

Mohanty, S., Ramsay, J.G., 1994. Strain partitioning in ductile shear zones: an example from a lower pennine nappe of Switzerland. Journal of Structural Geology 16, 663–676.

Ramberg, H., 1975. Particle paths, displacement and progressive strain applicable to rocks. Tectonophysics 28, 1–37.

Ramsay, J.G., 1980. Shear zone geometry: a review. Journal of Structural Geology 2, 83–99.

Ramsay, J.G., Graham, R.H., 1970. Strain variation in shear belts. Canadian Journal of Earth Sciences 7, 786–813.

Ramsay, J.G., Huber, M.I., 1987. The Techniques of Modern Structural Geology. Volume 2: Folds and Fractures. Academic Press, London, pp. 309–700.

Ring, U., 1999. Volume loss, fluid flow, and coaxial versus noncoaxial deformation in retrograde, amphibolite facies shear zones, northern Malawi, east-central Africa. Geological Society of America 111, 123–142.

Sanderson, D.J., Marchini, W.R.D., 1984. Transpression. Journal of Structural Geology 6, 449–458.

Simpson, C., 1983. Displacement and strain patterns from naturally occurring shear zone terminations. Journal of Structural Geology 5, 496–506.

Tikoff, B., Teyssier, C., 1994. Strain modeling of displacement — field partitioning in transpressional orogens. Journal of Structural Geology 16, 1575–1588.

Truesdell, C., 1954. Kinematics of vorticity. Indiana University Publications Science Series No. 19, Bloomington.